Geosci. Model Dev. Discuss., 5, 3375–3418, 2012
www.geosci-model-dev-discuss.net/5/3375/2012/
doi:10.5194/gmdd-5-3375-2012

Geoscientific Model Development Discussions

Stable water isotopes in the coupled atmosphere–land surface model ECHAM5-JSBACH

B. Haese, M. Werner, and G. Lohmann

Alfred Wegener Institute for Polar and Marine Research (AWI), Bussestr. 24, 27570 Bremerhaven, Germany

Received: 26 September 2012 – Accepted: 17 October 2012 – Published: 25 October 2012

Correspondence to: B. Haese (barbara.haese@awi.de)

Published by Copernicus Publications on behalf of the European Geosciences Union.

Abstract

In this study we present first results of a new model development, ECHAM5-JSBACH-wiso, where we have incorporated the stable water isotopes $H_2{}^{18}O$ and HDO as tracers in the hydrological cycle of the coupled atmosphere–land surface model ECHAM5-JSBACH. The ECHAM5-JSBACH-wiso model was run under present-day climate conditions at two different resolutions (T31L19, T63L31). A comparison between ECHAM5-JSBACH-wiso and ECHAM5-wiso shows that the coupling has a strong impact on the simulated temperature and soil wetness. Caused by these changes of temperature and the hydrological cycle, the $\delta^{18}O$ in precipitation also shows variations from −4.5 ‰ up to 4.5 ‰. One of the clearest anomalies is shown over North-East Asia where, depending on an increase of temperature, the $\delta^{18}O$ in precipitation increases as well. In order to analyze the sensitivity of the fractionation processes over land, we compare a set of simulations with various implementations of water isotope fractionation processes over the land surface. The simulations allow us to distinguish between no fractionation, fractionation included in the evaporation flux (from bare soil) and also fractionation included in both evaporation and transpiration (from water transport through plants) fluxes. The simulated $\delta^{18}O$ and δD in precipitation of these setups generally fit well with the observations and the best agreement between observation and simulation is given in the case where no fractionation over land surface is assumed.

1 Introduction

Since Dansgaard (1964) explored the coherence between the isotopic composition of $H_2{}^{16}O$, $H_2{}^{18}O$, and HDO in precipitation and climate variations, stable water isotopes have proven to be a useful tool for understanding climate variations and climate changes in the past. The composition of stable water isotopes as recorded in various paleoclimate archives (e.g. in ice cores, sediment cores, corals, tree-rings, or speleothems) have been used to reconstruct temperature and other climate changes

GMDD
5, 3375–3418, 2012

of the past. This is possible as the stable water isotopes differ by their mass and symmetry of their molecules. As a result, they behave differently at any phase transition of a water mass within the hydrological cycle on Earth. While the heavier molecules $H_2{}^{18}O$ and HDO tend to stay in the liquid or solid phase, the lighter $H_2{}^{16}O$ molecules evaporate more easily. The strength of this partitioning effect, called fractionation, depends on the surrounding environmental conditions, with temperature as one of its key influencing parameters.

However, the interpretation of the isotope proxy data (usually expressed in a δ-notation) is often not straight forward, because the proxy data includes a mixture of fractionation processes occurring during evaporation (from bare soil or open water bodies) and transpiration (through plants) of liquid water, mixing of water masses of different origin and fractionation during condensation processes leading to the final isotopic composition of precipitation. Furthermore, the measured isotopic signal may also be affected by local post-depositional surface processes, e.g. for terrestrial archives by river runoff or percolation through the soil, or for ice cores by wind erosion or sublimation.

After the pioneering work by Joussaume et al. (1984), several atmospheric general circulation models (AGCMs) were enhanced with modules for modeling stable water isotopes in the hydrological cycle (e.g. Jouzel et al., 1987; Hoffmann et al., 1998; Noone and Simmonds, 2002; Lee et al., 2007; Risi et al., 2010; Werner et al., 2011). Further oceanic GCMs (Schmidt, 1998; Xu et al., 2012), coupled atmosphere-ocean models (Schmidt et al., 2007; Tindall et al., 2009), land surface schemes (Fischer, 2006; Yoshimura et al., 2006), as well as coupled land surface-atmosphere models (Aleinov and Schmidt, 2006) have also been enhanced with modules of stable water isotopes. A detailed overview about the existing GCMs enhanced with an isotope module is given by Sturm et al. (2010).

An enormous benefit of modeling stable water isotopes is the ability to directly compare field data to modeled isotope data. Thus, the models can be evaluated with present day observational data found for example in the GNIP (Global Network of Isotopes in Precipitation) database (IAEA/WMO, 2006). Furthermore, the interpretation

GMDD
5, 3375–3418, 2012

of the measured variations of isotopes can be supported by model simulations. Studies like those of Jouzel et al. (2000), Vuille and Werner (2005), Herold and Lohmann (2009), and Risi et al. (2010) show that the interpretation of proxy data benefits from the addition of isotope modeling.

Over land surfaces two main processes exist which include a phase transition of water masses: evaporation and transpiration. Whereas isotope fractionation occurs during an evaporation process, it is often assumed that the transpiration is a non-fractionating process (see Gat, 1996). Many of the presently existing GCMs enhanced with isotopes do not consider such difference between the evaporation and transpiration flux but simply assume that the whole evapotranspiration from land surface is a non-fractionating process (see, e.g. Hoffmann et al., 1998, for a more detailed discussion of this issue). So far, only very few GCM studies, e.g. Aleinov and Schmidt (2006), have started to investigate fractionation processes over land.

In this study, we present the first results of a newly developed isotope scheme within the ECHAM5-JSBACH model (named ECHAM5-JSBACH-wiso hereafter). The model is built from two separate components, the atmosphere model ECHAM5 (Roeckner et al., 2003) and the land surface scheme JSBACH (Jena Scheme for Biosphere-Atmosphere Interaction in Hamburg, Raddatz et al., 2007). The atmosphere isotope processes in this coupled model are almost identically implemented as in the stand-alone ECHAM5-wiso model version (Werner et al., 2011), while the isotopic diagnostics within land surface processes are a novel development within JSBACH. With this setup it is possible to distinguish between the two partial fluxes of evapotranspiration, evaporation and transpiration, and separately incorporate the relevant fractionation processes for both fluxes.

We focus in our study on two questions: first, what are the implications of using ECHAM5-JSBACH-wiso instead of ECHAM5-wiso? Here we examine key variables of JSBACH, which can influence the atmospheric water cycle in ECHAM5, and the related changes of the isotopic composition of precipitation. Secondly, how sensitive are the isotope results of ECHAM5-JSBACH-wiso to different assumptions regarding the

GMDD
5, 3375–3418, 2012

fractionation processes over land. In general, any isotopic fractionation during evaporation consists of two parts: an equilibrium fractionation occurring between the liquid water and a thin, saturated vapor layer above the water mass, plus a kinetic fractionation process occurring during the diffusion of the water molecules from the saturated vapor layer into the undersaturated free atmosphere (Gat, 1996). For the equilibrium fractionation we perform sensitivity studies to distinguish between three different approaches. First, we assume that no fractionation during evapotranspiration occurs at all, similar to the approach used in the ECHAM5-wiso model (Werner et al., 2011). Second, we assume that fractionation only occurs during evaporation from bare soil but not during transpiration. Last, we consider that fractionation processes take part during both evaporation and transpiration of water from land surface. For the impact of the kinetic fractionation factor, we additionally analyze two different formulations given by Merlivat and Jouzel (1979) as well as Mathieu and Bariac (1996).

In the following section we give a detailed description of the ECHAM5-JSBACH-wiso model. Furthermore we explain the performed set of simulations as well as the selection of observational data for evaluating the model results. The comparison of ECHAM5-JSBACH-wiso and ECHAM5-wiso follows in Sect. 3.1. In Sect. 3.2 we investigate the sensitivity of the impact of fractionation over land, and distinguish between the equilibrium fractionation and the relevance of the kinetic fractionation factor. The final section of this manuscript includes the conclusion and an outlook.

2 Model description, simulation setup and observational data

2.1 Model description

ECHAM5 is an atmosphere general circulation model (AGCM), developed mainly at the Max Planck Institute for Meteorology, Hamburg, that consists of a spectral, dynamical core based on the equations of conservation of momentum, mass and energy. This set of equations is completed by the hydrostatic equation, the continuity equation,

GMDD
5, 3375–3418, 2012

and a prediction equation for the surface pressure (Roeckner et al., 2003). The hydrological cycle in the model consists of the formulations for evaporation of ocean water, evapotranspiration from terrestrial water, two schemes for the formation of large scale and convective clouds, as well the independent advective transport of vapor, liquid and frozen water within the atmosphere. A detailed description of the physics of the model as well as changes to the earlier model version can be found in Roeckner et al. (2003).

During each time step the JSBACH model calculates the terrestrial boundary conditions for ECHAM5 over the land surface. This includes a simulation of the exchange of energy, water, momentum, and CO_2 between the land surface and the atmosphere. JSBACH is based on the ECHAM3 soil model (DKRZ, 1992) and the biosphere model "Biosphere Energy Transfer and Hydrology scheme", called BETHY (Knorr, 2000). The basic idea of the model structure is a partitioning of the land surface. Each grid cell includes various tiles, which represent the fraction covered by one of the plant functional types (PFTs), as well as a fraction of bare soil. In our version of JSBACH (Raddatz et al., 2007) there are 8 PFTs implemented, which can distinguish between tropical and nontropical as well as deciduous and evergreen trees, deciduous and evergreen shrubs, C3 grasses, and C4 grasses, as well as one type for seasonally bare soil and one for permanently bare soil (i.e. desert). The simulated vegetation is based on temporal change of growing, natural mortality, and disturbance mortality (e.g. wind, fire). The modeling of vegetation and its dynamics are explained in detail by Brovkin et al. (2009).

As in the stand alone atmosphere model ECHAM5-wiso the water isotope tracers in ECHAM5-JSBACH-wiso are implemented parallel to the normal water cycle. Fractionation of $H_2{}^{18}O$ and HDO versus $H_2{}^{16}O$ occurs during any phase change. Aside from fractionation during evapotranspiration from the land surface, all fractionation processes in ECHAM5-JSBACH-wiso are implemented in an identical manner to ECHAM5-wiso. For evaporation over the ocean, we use the bulk formula described by Hoffmann et al. (1998). This equation includes the dependence of the isotope evaporation flux on the isotopic compositions of water vapor close to the ocean surface, evaporation

GMDD
5, 3375–3418, 2012

temperature, relative humidity, and wind speed at the ocean surface (Hoffmann et al., 1998). The implementation of fractionation processes inside the cloud schemes, specifically during cloud formation, are described in detail by Werner et al. (2011). Furthermore, as in ECHAM4-wiso we use the assumption that convective showers generate primarily large raindrops equilibrating isotopically to only 45 % as they fall through an undersaturated atmosphere, and that large-scale clouds generate smaller rain drops equilibrating nearly completely (95 %) with its surrounding (see Hoffmann et al., 1998 for details).

Over land, three surface water reservoirs, wich can be evaporated or transpired, are implemented in the JSBACH model: a snow layer (sn), a soil water layer (ws) and water at the skin layer of the canopy (wl). Each of these reservoirs has its own ratio of water isotopes $R^x_{\text{reservoir}}$ with $x \in \left\{ H_2^{16}O,\ H_2^{18}O,\ HDO \right\}$. We assume that fractionation only takes place in the soil reservoir. This assumption is based upon the physical properties of the other two reservoirs. For the snow reservoir sn, no fractionation occurs during sublimation due to the low diffusion rate in the ice crystal structure. The skin layer wl is modeled as a thin layer of water on top of the vegetation canopy, which in general evaporates completely within a few model time steps. If this entire water reservoir is evaporating, no fractionation of different isotopes can occur and thus, the evaporation flux has an identical isotopic composition as the water source.

Water from the soil reservoir ws, can either evaporate (E) from bare soil or transpire (T) through the vegetation. Since the soil water layer of JSBACH is implemented as a simple one-layer bucket model, the corresponding soil water reservoir for the isotopes also has only one layer. The evaporation flux from the soil reservoir is calculated as:

$$E_{\text{ws}} = F_{\text{bs}}\, \rho\, C_V\, |\boldsymbol{v}_{\text{h}}|\, \left(q_{\text{vap}} - h\, q_{\text{sat}} \right). \tag{1}$$

Analogously the equation for transpiration is formulated as:

$$T = F_{\text{veg}}\, \frac{\rho\, C_V\, |\boldsymbol{v}_{\text{h}}|}{1 + C_V\, |\boldsymbol{v}_{\text{h}}|\, S}\, \left(q_{\text{vap}} - q_{\text{sat}} \right). \tag{2}$$

GMDD
5, 3375–3418, 2012

Here q_{sat} is the saturated specific humidity at the corresponding temperature, q_{vap} is the humidity of the air level direct above surface, h is the relative humidity, $\boldsymbol{v}_h$ is the horizontal wind speed at the surface, C_V is the drag coefficient for water flux, ρ is the density of air, F_{bs} or F_{veg} is the fraction of ws without or with vegetation, and S includes the stomata resistance as well as the factor for water stress. In case of a negative flux the model simulates evaporation and transpiration, in case of a positive E flux Eq. (1) represents the formation of dew.

To calculate the fractionation during evaporation and transpiration, we use the equilibrium fractionation factor $\alpha^x(T)$ obtained from Majoube (1971a) and Majoube (1971b), and a factor for kinetic fractionation (α_k). The evaporation from bare soil enhanced with fractionation is described by:

$$E^x_{res} = R^x_{res}\, F_{bs}\, \rho\, C_V\, |\boldsymbol{v}_h|\, \alpha_k \left(q^x_{vap} - \alpha^x(T)\, h\, q_{sat}\right). \quad (3)$$

Here R^x_{res} represents the mixing ratio of the isotopes for a specific source given by res (soil water or moisture at the lowest air layer). Analogously the formula for transpiration with fractionation is given by:

$$T^x_{ws} = R^x_{ws}\, F_{veg}\, \frac{\rho\, C_V\, |\boldsymbol{v}_h|}{1 + C_V\, |\boldsymbol{v}_h|\, S} \left(q^x_{vap} - \alpha^x(T)\, q_{sat}\right). \quad (4)$$

The term α_k in Eq. (3) includes the non-equilibrium fractionation effects, taking into account the kinetics during the diffusion of vapor from a thin layer just above the soil water into the free atmosphere. For the calculation of the kinetic fractionation two different approaches are tested. First, one can use for evaporation over land the same kinetic fractionation factor as for evaporation over the ocean. The latter has been described by Merlivat and Jouzel (1979). The second approach is given by Mathieu and Bariac (1996), in which the kinetic fractionation is a function dependent on the diffusion resistance. The impact of these two different kinetic fractionation factors on the isotopic composition of the different modeled water reservoirs is analyzed and discussed in detail in Sect. 3.2.3.

GMDD
5, 3375–3418, 2012

2.2 Simulation setup

All simulations are run under present day conditions with a prescribed present day vegetation over a simulation period of 10 yr after a spin-up period of 2 yr. We distinguish between the model resolutions T31L19 (horizontal grid size 3.8° × 3.8°, 19 vertical model levels) and T63L31 (1.8° × 1.8°, 31 levels). The simulations are performed with AMIP-conform present-day boundary conditions including prescribed climatological sea surface temperatures and sea ice cover for the period 1979–1999 (see Taylor et al., 2000). Moreover, we also use a prescribed present-day vegetation distribution. The lower oceanic boundary condition for the atmospheric ^{18}O isotopic composition is based on the dataset described by LeGrande and Schmidt (2006). This is a global gridded dataset for sea surface water and sea ice. As no equivalent dataset is available for the composition of HDO we use as lower oceanic boundary condition for the isotopic composition of deuterium the observed relation for meteoric water on a global scale (Craig and Gordon, 1965) and assume $\delta D = 8 \cdot \delta^{18}O$ for sea surface water and sea ice.

To evaluate the sensitivity of the fractionation processes over land we use a set of present-day simulations with various fractionation schemes implemented. The fractionation process over land will be varied between no fractionation (simulation named noF), fractionation occurring during evaporation only (FE), and fractionation occurring during both evaporation and transpiration (FET). These three cases are all performed without any additional kinetic fractionation ($\alpha_{kin} = 1$). To investigate the influence of the kinetic fractionation of terrestrial evaporation on the isotopic composition of the different water reservoirs we use the FE fractionation scheme extended by two different calculations of the kinetic fractionation factor α_{kin}. The first setup, called $FEK_{openwater}$, uses the same kinetic fractionation factor over land surface as over the ocean (as given by Merlivat and Jouzel, 1979). The second setup calculates α_{kin} in dependence on the diffusion resistance, as proposed by Mathieu and Bariac (1996). This setup is called $FEK_{diffres}$.

GMDD
5, 3375–3418, 2012

For a comparison of the ECHAM5-JSBACH-wiso results with the stand-alone ECHAM5-wiso model, we use two comparable present day ECHAM5-wiso control simulations in T31L19 and T63L31 resolution, from Werner et al. (2011).

2.3 Observational data

As observational data for evaluating the model results we choose the Global Network of Isotopes in Precipitation (GNIP) database. Since 1961, the International Atomic Energy Agency (IAEA) and the World Meteorology Organization (WMO) have collected monthly precipitation samples at more than 800 meteorological stations in 101 countries. Additional information and the available data can be found in IAEA/WMO (2006). For this study we choose 248 GNIP stations where isotope data has been recorded for at least three consecutive years within the time period 1961 to 2008, and where at least 10 months of data per year are available. As a further restriction, we only use stations, which provide a full monthly mean data set, including values of 2 m air temperature (T_{2m}), precipitation amount (P), and the isotopic composition of precipitation ($\delta^{18}O_P$ and δD_P). We are aware that three years is a perhaps too short period to represent a long-term climatological mean value at the stations' locations. On the other hand there are only 74 GNIP stations which have collected 10 yr or more of data. Since most of them are located in Central Europe, many regions in Asia, America, Africa, and Australia would be underrepresented in such a limited data set. Therefore we opted for a three-year time period in order to be able using a globally more representative sample distribution.

GMDD
5, 3375–3418, 2012

3 Results and discussion

3.1 Impact of the coupling from ECHAM5 and JSBACH

In order to get an impression of how the overall model results change by using ECHAM5-JSBACH-wiso instead of ECHAM5-wiso we first compare the simulated surface temperature, precipitation amount, and soil wetness results of both models. All these variables are independent of the isotope diagnostic scheme, and differences between simulation results of both models are related to the changed representation of land surface processes in ECHAM5-JSBACH as compared to the stand-alone ECHAM5 model. Then, we take a look at the simulated distribution of $\delta^{18}O$ in precipitation (here after named $\delta^{18}O_P$). As no fractionation for evaporation and transpiration processes has been assumed in the ECHAM5-wiso model by Werner et al. (2011), we use the analogous ECHAM5-JSBACH-wiso setup (noF) for this comparison.

3.1.1 Surface temperature, precipitation amount, and soil wetness

Figure 1a and c shows the mean annual temperature and soil wetness as simulated by ECHAM5-JSBACH-wiso for the model resolution T31L19. The corresponding anomaly as compared to the comparable ECHAM5-wiso simulation is pictured in Fig. 1b, d. The modeled temperature difference varies from a −2.7°C and −1.4°C decrease over Antarctica and Greenland to a warming of +0.5°C to +2°C over Eurasia and North-America. The strongest change is shown in North-East Russia with +2.1°C. These temperature changes are strongly related to the variation of the simulated surface albedo (Fig. 2a), which shows an increase over Antarctica as well as Greenland and a decrease over North America and Eurasia. For the finer model resolution T63L31 (not shown) most of the anomaly patterns are similar with two exceptions. First, the Caspian Sea region shows a cooling of −0.5°C to −1°C, due to a change in the local albedo. Second, a cooling of similar magnitude is also seen over Australia, despite the fact that both resolutions show a comparable albedo level over this region. However,

GMDD
5, 3375–3418, 2012

while the simulated surface temperature in the T31L19 resolution shows a warming over Australia, which could be related to the decrease of the simulated albedo anomaly in South-West Australia, the simulated temperature anomaly in the resolution T63L31 shows the same pattern as the simulated surface albedo difference, a warming in South-West Australia and a cooling everywhere else in Australia.

The simulated soil wetness differs between both models as well (Fig. 1d). The most notable changes are in the Amazon region, where an increase of 20 cm is present, and in South Africa, where a decrease of 0.25 cm can be seen. There is also a clear increase in a range of 0.08 cm to 0.15 cm over the Sahara. Locations displaying a decrease in soil moisture generally show also an increase of evapotranspiration, which can be linked to changes in the simulated surface temperature. Contrastingly, for the Amazon region and Saharan Africa a larger maximal depth of the soil layer (Fig. 2b) is prescibed as a boundary condition in ECHMA5-JSBACH-wiso as compared to ECHAM5-wiso, which most likely explains the simulated soil wetness increases. For the finer resolution T63L31, differences in the simulated soil wetness can be also detected. The increase of soil wetness in the Amazon Basin present at T31L19 is no longer seen at T63L31. This is probably caused by an identical prescribed maximal soil layer depth in ECHAM5-JSBACH-wiso and ECHAM5-wiso for the T63L31 resolution. A second change between the ECHAM5-JSBACH-wiso and ECHAM5-wiso simulation is seen in a slight increase of soil wetness over North-East Australia (approx. 5 to 10 cm), which might be related to the observed cooling of surface temperature. Furthermore less evapotranspiration occurs over North-East Australia in the higher resolution model.

The simulated mean annual precipitation amount (not shown) shows nearly the same pattern in both models. While there are only some minor shifts of the precipitation pattern in the tropics for the T31L19 resolution, less precipitation in range of 30–60 mm month^{-1} (which corresponds to 0.5 %–4 % of the annual mean precipitation amount) simulated over middle and South Africa and over India in the T63L31 simulatation.

GMDD
5, 3375–3418, 2012

3.1.2 Isotopic compositions of precipitation and soil water

Figure 3 shows the simulated $\delta^{18}O$ in precipitation ($\delta^{18}O_P$) using the noF setup (no fractionation during evaporation and transpiration) of ECHAM5-JSBACH-wiso model for both model resolutions, T31L19 (Fig. 3a) and T63L31 (Fig. 3b). Both simulations show the typical $\delta^{18}O_P$ pattern described by Dansgaard (1964). We see a depletion from the tropics to the high latitudes (temperature effect) as well as a depletion from the oceans to the landmasses of North-America and Eurasia (continental effect). A depletion of $\delta^{18}O_P$ above the mountain areas can also be identified (altitude effect), for example for the Andes. However, Fig. 3b also shows that the altitude effect is better represent in the higher model resolution T61L31. The root mean square error (RMSE) between the simulations and the GNIP data is 2.23 ‰ for T31L19 and 1.76 ‰ for T63L31, which shows that the simulated $\delta^{18}O_P$ values improve for a higher ECHAM5-JSBACH-wiso model resolution. For the analogue simulations with the ECHAM5-wiso model the calculated RMSE with respect to the same set of GNIP stations is 2.22 ‰ for T31L19 and 1.89 ‰ for T63L31. Thus, both models show similar results for $\delta^{18}O_P$ on a global scale.

In order to further analyze the impact of the coupling of ECHAM5 with JSBACH for the simulation of stable water isotopes, we calculate the difference of $\delta^{18}O_P$ between ECHAM5-JSBACH-wiso and the ECHAM5-wiso simulations for both resolutions (Fig. 4). Due to the relative short simulation period of 10 yr, we exclude in our analyses $\delta^{18}O_P$ changes in the range of −1 ‰ to +1 ‰, as such small differences might be caused by internal model variability, only. The strongest differences with an increase of approx. +4 ‰ are located in the Sahara Dessert (for both resolutions) and along the coast of Antarctica (for resolution T63L31). The changes in the Sahara can be related to an decrease in the amount of precipitation or an increase of soil wetness. In Antarctica, the changes are most likely due to different temperatures simulated in this region. A further change of $\delta^{18}O_P$ is evident in North-East Russia where the strongest temperature increase was detected (see Fig. 1b). As expected, this temperature increase causes

GMDD
5, 3375–3418, 2012

an enrichment of $\delta^{18}O_P$ in both resolutions. Over Australia the two resolutions show opposite anomalies in $\delta^{18}O_P$. For the T31L19 resolution ECHAM5-JSBACH-wiso simulates heavier rainfall than ECHAM5-wiso (approx. 1 ‰ to 1.5 ‰), while for the T63L31 resolution, the model simulates isotopically lighter precipitation. These differences can be linked to the changes of surface temperature and soil wetness between the two resolutions.

For a further model evaluation we investigate the relationship between $\delta^{18}O$ and 2 m temperature above the surface ($\delta^{18}O - T_{2m}$) as well as $\delta^{18}O$ and the amount of precipitation ($\delta^{18}O - P$). For the $\delta^{18}O$-temperature relationship we use those 186 GNIP stations, where the annual mean temperature is below 20 °C. Figure 5 shows the simulated $\delta^{18}O - T_{2m}$ relation for both ECHAM5-JSBACH-wiso and ECHAM5-wiso. Both models show a similar $\delta^{18}O - T_{2m}$ relation as derived from the GNIP data, but slightly overestimate $\delta^{18}O_P$. The simulated strong correlation between $\delta^{18}O$ and T_{2m} in ECHAM5-JSBACH-wiso is statistically significant for both model resolutions (Pearson Correlation coefficient: $R^2 = 0.894$ for T31 and $R^2 = 0.921$ for T63), similar to the observed correlation at the GNIP stations ($R^2 = 0.909$). As seen in Fig. 5, the simulated $\delta^{18}O - T_{2m}$ relation also slightly improves for the finer model resolution T63L31. Additionally, the correlation of $\delta^{18}O$ and precipitation is analyzed. For this comparison we choose the other 62 GNIP stations with a mean annual temperature above or equal to 20 °C. The simulated relation fits quite well to the observed relation for both model resolutions (Fig. 6) with a slight tendency to underestimate the $\delta^{18}O - P$ relation in the T31L19 resolution (both ECHAM5-wiso and ECHAM5-JSBACH-wiso). We refrain from a more quantitative analysis of the simulated $\delta^{18}O - T_{2m}$ and $\delta^{18}O - P$ relation in this study as both the simulated and observed mean $\delta^{18}O_P$, T, and P values may contain relatively large uncertainties due to the short simulation (10 yr) and GNIP observation (3 yr or more) period.

In summary, the analyses show that the coupling of the atmosphere model ECHAM5 with the surface scheme JSBACH has a strong impact on the simulated temperature,

GMDD
5, 3375–3418, 2012

evapotranspiration, and soil wetness. These changes are related to the alteration in the simulated surface albedo parameters and the prescribed maximum soil wetness. The simulated precipitation is less strongly influenced by the coupling. Since the isotopic composition of precipitation highly depends on these variables, the coupling of ECHAM5 with JSBACH also has a strong impact on the simulated $\delta^{18}O_P$ values in various regions. However, our analyses also reveal that the ECHAM5-JSBACH-wiso model is capable of simulating a global distribution of $\delta^{18}O_P$ in a good overall agreement with available observations from GNIP stations, similar to previous results retrieved with the stand-alone ECHAM5-wiso model.

3.2 Fractionation processes over land surfaces

In this section we investigate the sensitivity of the ECHAM5-JSBACH-wiso simulation results regarding different assumptions for both the equilibrium fractionation (Sect. 3.2.1) as well as the kinetic fractionation (Sect. 3.2.3) over land surface. All simulations in this part of our study are performed at resolution T31L19, and it should be kept in mind that the simulation of the various water isotope values generally becomes better at higher model resolutions, as already shown in detail by Werner et al. (2011).

3.2.1 Equilibrium fractionation during evaporation and transpiration

When water evapotranspirates from the soil compartment, it can either evaporate from bare soil or transpire through the vegetation. According to Wang and Dickson (2012), transpiration is the largest contribution to evapotranspiration on a global scale. This relevance of transpiration is also seen in the ECHAM5-JSBACH-wiso simulations. In Fig. 7 the modeled annual mean evapotranspiration flux from land surface and the fraction of evaporation in relation to the total evapotranspiration flux is shown. Especially in the (sub)tropical regions, transpiration is the dominant water flux from land surface

GMDD
5, 3375–3418, 2012

to the atmosphere, while evaporation dominates over transpiration mainly in northern high latitude regions as well as the Tibetan Plateau.

For the incorporation of stable water isotopes in GCMs or land surface schemes various assumptions for the description of the equilibrium fractionation process during evapotranspiration have been utilized. Studies like the one by Yoshimura et al. (2006) assume a fractionation during transpiration while others such as Fischer (2006) assume no fractionation during transpiration. Recent studies like the one by Sachse et al. (2012), which investigates the hydrogen-isotopic composition of leaf water, indicate that the real situation occuring in nature lies somewhere in between these two extremes. Thus, for our sensitivity studies we assume both extreme cases for transpiration as well as a third case comparable to many previous GCM studies: for one model setup (named FE) we assume isotope fractionation during evaporation processes, only, and for another setup (FET) we assume isotope fractionation during both evaporation and transpiration. By a third setup (noF) we examine the case if no fractionation occurs during evaporation and transpiration, at all.

Figure 8a, b show the simulated difference in $\delta^{18}O_P$ for the three setups. When using the FE setup instead of the noF one (Fig. 8a), a weaker depletion of the modeled annual mean $\delta^{18}O_P$ over land in the range of −6 ‰ to −1 ‰ is dedected. A similar pattern is seen for the simulation of HDO (not shown) with differences of δD_P in the range of −48 ‰ to −8 ‰. The area with the strongest enrichment of $\delta^{18}O_P$ is Eurasia, particularly in the area of Tibet. The anomaly plot of noF–FET (Fig. 8b) reveals a stronger depletion of $\delta^{18}O_P$ for the noF setup relative to the FET setup, as well, yet the difference is less than for the FE setup. The maximum change is found over Tibet with a stronger depletion for the noF case of −4.5 ‰ in $\delta^{18}O_P$ (−37 ‰ in δD_P), and over most areas the anomalies vary between −3 ‰ to −1 ‰ (−25 ‰ to −8 ‰). The reason for the weaker increase of $\delta^{18}O_P$ (δD_P) in FET as compared to FE is a modeled isotopic enrichment of the soil reservoir (see Fig. 9). Since in the FET setup the entire evapotranspiration flux fractionates, the soil reservoir becomes more enriched in comparison to the FE setup.

GMDD
5, 3375–3418, 2012

The difference of the modeled annual mean $\delta^{18}O_{ws}$ between the noF–FE and the noF–FET setup, respectively, is shown in Fig. 9. For the comparison of noF and FE (Fig. 9a) we see a relative stronger depletion of $\delta^{18}O_{ws}$ in the noF setup from −1 ‰ to −9 ‰ over the land mass in the region of North Africa via the Arabian Peninsula to the Tibetan Plateau, South Africa, Australia and the areas of Rocky Mountains and Andes Mountains. In all other areas the $\delta^{18}O_{ws}$ in the FE setup is stronger depleted than in the noF setup with differences in a range of 1 ‰ to 6 ‰. The difference between noF–FE setup of the simulated annual mean $\delta^{18}O$ in the net precipitation (not shown), which has been estimated as precipitation minus evaporation, results in a very similar pattern like for soil wetness over land surface. Furthermore, at the areas where the simulations of the FE setup result in relatively less depletion in comparison to the noF setup, the simulated mean annual net precipitation is approx. zero, in all other areas there is a positive net precipitation. Therefore, the relative stronger depleted $\delta^{18}O_{ws}$ in the simulated soil wetness in the FE setup, like, e.g. in Europe, can be linked to the also stronger depleted modeled net precipitation, which is the source for the soil water. For the comparison of noF and FET (Fig. 9b) we see a relative stronger depletion of $\delta^{18}O_{ws}$ in the noF setup from −2 ‰ to −6 ‰ over the land mass in the tropics and mid latitudes, while in the high northern latitudes a relative enrichment from 1 ‰ to 8 ‰ is observed. However, the simulated difference of $\delta^{18}O_{ws}$ of noF–FET also show the same pattern like the anomaly of the simulated annual mean $\delta^{18}O$ in the net precipitation.

Next, we analyze how accurately the different setups FE, FET, and noF simulate $\delta^{18}O$ values in precipitation as compared to the various present-day GNIP observations. Figure 10 shows a comparison of the simulated $\delta^{18}O_P$ and the observations from the set of 248 GNIP stations described in Sect. 2.3. We distinguish again between GNIP data of stations with a mean annual temperature $T \leq 20^{\circ}C$ (Fig. 10a) and those stations with a mean annual temperature $T \geq 20^{\circ}C$ (Fig. 10b). For all three model setups, the calculated correlation between simulated and observational values is significant for $\delta^{18}O_P$ and δD_P (see Table 1). Moreover, we find for GNIP stations with $T \leq 20^{\circ}C$ that the noF setup results in $\delta^{18}O_P$ values closest to the observations

GMDD
5, 3375–3418, 2012

(Fig. 10a). However, Fig. 10a also shows that all three simulations overestimate $\delta^{18}O_P$ for most of these GNIP stations. A slightly different result is found for GNIP stations with $T \geq 20^{\circ}C$ (Fig. 10b). For these stations, $\delta^{18}O_P$ is in numerous cases underestimated in the noF setup, but again more enriched for the two setups which include isotope fractionation.

3.2.2 Seasonal changes

In order to get a more detailed picture regarding the modeled isotope variations, we analyze the seasonal cycle of the simulations using the FE, FET, and noF model setup. For this purpose we choose nine GNIP stations from different geographical positions where the seasonal cycle of vegetation, amount of precipitation, temperature and the influence of evaporation over land strongly varies and compare the ECHAM5-JSBACH-wiso results to these GNIP data.

The first two stations are located on islands, where the influence of evaporation from the land surface is negligible in comparison to evaporation from the surrounding ocean. The station Reykjavik is chosen to represent the high northern latitudes and the GNIP station in Jakarta represents the tropics. Since the only distinguishing factor between the three model setups is the fractionation of evapotranspiration over land, one can assume, that the model behaves the similarly in all implementations for the selected islands. For Reykjavik (Fig. 11a) all simulations reveal a correct seasonal timing of temperature, precipitation, and $\delta^{18}O_P$, but the simulated $\delta^{18}O_P$ shows an enrichment off +2 ‰ in the FE and FET setup in comparison to the noF setup. The reason for this difference is a non-negligible local evapotranspiration flux from the land surface, which has a fraction of evaporation in the range of approx. 60 % to 85 %. For Jakarta (Fig. 11b) the simulated evaporation and transpiration from land as well as the simulated soil wetness are zero. For the surface temperature, there is a good agreement between the simulated and observed values in Jakarta, while the simulated precipitation is strongly overestimated in the period April till Juli. The $\delta^{18}O_P$ has a correct timing of the seasonal

GMDD
5, 3375–3418, 2012

cycle, but slightly too enriched values in fall. For all three model setups the simulated $\delta^{18}O_P$ is very similar.

Because some of the strongest difference in $\delta^{18}O_P$ and $\delta^{18}O_{ws}$ between the different ECHAM5-JSBACH-wiso sensitivity experiments takes place in North America and Eurasia (as seen in Figs. 8 and 9) we choose three stations of these regions for comparison: Vienna, Ottawa, and Yakutsk. At all these locations, strong seasonal variations of vegetation and temperature exist, but the amplitude of the temperature varies strongly. At Vienna (Fig. 12a), the simulated temperature fits well with the observations, but the simulated precipitation shows a overestimation during the late fall and winter. For all three model setups, the $\delta^{18}O_P$ is also overestimated. While the noF setup shows the correct seasonality but a slight offset in the range of +1‰ to +2‰ as compared to the GNIP values, the other simulations based on the FE and FET setup produce very enriched $\delta^{18}O_P$ values in winter and fall. These deviations are highly correlated to the simulated fraction of local evaporation, which increases strongly between November and April. The simulated temperature also fits well in Ottawa (Fig. 12b), however all simulation setups overestimate the seasonality of precipitation. For $\delta^{18}O_P$, the simulations results have a correct seasonal timing, but all simulations overestimate the seasonal $\delta^{18}O_P$ amplitude, especially in summer. For Yakutsk, all simulations reveal a correct timing of the seasonality for temperature, preciptation, and $\delta^{18}O_P$ (Fig. 12c). While the seasonal amplitude of temperature and $\delta^{18}O_P$ agrees well with the GNIP observations, the ECHAM5-JSBACH-wiso model simulates too much summer precipitation in this region. For the noF, FE, and FET model setups, the simulated $\delta^{18}O_P$ is very similar, but with a minor difference of approx 2–3‰ between the simulations in summer and early fall. By comparison of the simulated soil wetness for the three GNIP stations Vienna, Ottawa, and Yakutsk differences in the amplitude can be detected. So is the calculated amplitude in soil wetness for Vienna approx. 15 cm, for Ottawa approx. 7 cm, and for Yakutsk only 2 cm. Furthermore, the time interval in which transpiration takes place varies for these three stations, the longest, with March to November, is

GMDD
5, 3375–3418, 2012

simulated for Vienna, a similar range (April to November) is simulated for Ottawa, and for Yakutsk only a interval from June to October is calculated.

To analyze the model performance in arid areas or areas with strong seasonal precipitation changes, we examine the stations Alexandria (Fig. 13a), Bamako (Fig. 13b), Kinshasa (Fig. 13c), and Addis Ababa (Fig. 13d). Alexandria is located in a very arid area with a dry season between May and September. This dry season is well simulated in ECHAM5-JSBACH-wiso, but the winter precipitation in the model is underestimated. Both temperature and $\delta^{18}O_P$ agree well with the GNIP observations with a slight overestimation of the simulated $\delta^{18}O_P$. Furthermore, the ECHAM5-JSBACH-wiso simulates a very thin soil wetness layer (approx. 0.5 cm) as well as a very small evapotranspiration flux. The calculated $\delta^{18}O_{ws}$ differs strongly between noF with approx. −4 ‰ and FE respectively FET with approx. +2 ‰. For Bamako (Fig. 13b), the simulated precipitation and temperature fit well with the observations. The simulated $\delta^{18}O_P$ values are approximately the same for all implementations, with too depleted $\delta^{18}O_P$ values in the dry season between January and May as compared to the GNIP data. The peak of the summer depletion is simulated with a delay of one month, and the modeled $\delta^{18}O_P$ values are slightly overestimated during the rainy season for the FE and FET setup as compared to the noF setup. For the soil wetness depth, the ECHAM5-JSBACH-wiso model simulates a strong seasonality (from 0.45 m during the dry season to 0.9 m during the wet season), but the related $\delta^{18}O_{ws}$ values of the noF and FE setup display weak seasonal variations. Additionally, these two simulations have more or less the same $\delta^{18}O_{ws}$ values. Only for the FET setup, strong seasonal changes of $\delta^{18}O_{ws}$ are simulated. Similarly to the situation at Bamako, the monthly temperature and precipitation model results for Kinshasa (Fig. 13c) fit well to the observations. One major exception is an underestimation of the modeled precipitation amount in November. The simulation results reveal also a strong seasonality of the soil water (from 0.21 m during the dry season to 0.42 m during the wet season). The simulated $\delta^{18}O_{ws}$ values are different for the three sensitivity studies. While there exists no change of $\delta^{18}O_{ws}$ in the noF setup, a weak seasonal cycle is detected for the FE setup.

GMDD
5, 3375–3418, 2012

The FET results show a strong seasonal cycle, inversely correlated to the seasonality of ws. The modeled $\delta^{18}O_{ws}$ values for the FE setup are stronger depleted by 2–3‰ when compared to the noF setup. These differences of the noF and FE setup, in combination with the amount of evaporation, are directly imprinted in the simulated $\delta^{18}O_P$ values at the location Kinshasa. At Addis Ababa (Fig. 13d), the simulated temperature is overestimated by +3 °C to +5 °C. Modeled precipitation values have a correct seasonal timing, but the amount of summer precipitation is underestimated. The simulated soil wetness also shows a strong seasonality, which lags the seasonal cycle of precipitation by 3–4 months. The modeled $\delta^{18}O_{ws}$ values are almost constant in the noF setup, while the FE and FET setup, which include fractionation, show seasonal changes in $\delta^{18}O_{ws}$ inversely correlated to the seasonal cycle of soil wetness. In the FET case the $\delta^{18}O_{ws}$ values fluctuate around +0.5‰, and for the FE setup they vary around −4‰. In the model setups FE and FET the simulated seasonal cycle of $\delta^{18}O_P$ is inversed compared to the GNIP observations, while a decrease of $\delta^{18}O_P$ is simulated in the noF setup in the period from Mai till October.

The performed sensitivity studies reveal that the various simulation results with the ECHAM5-JSBACH-wiso model are in relatively good agreement with the GNIP observations, but in many cases the model overestimates the isotope values in precipitation. Including fractionation effects during the evaporation and/or transpiration of water from land surface does not improve the model results, but rather causes an even stronger enrichment of $\delta^{18}O_P$ for many locations. The reason for this mismatch is probably caused by the rather simple one-layer bucket model of soil water implementation in the coupled ECHAM5-JSBACH model. When using a simple bucket model for the soil water, the whole soil water reservoir does have an identical isotopic composition. Any vertical moisture dynamics and changes of the isotopic composition with the soil moisture depth are neglected. But it is well known from observations (see, e.g. Allison and Hughes, 1983, Hsieh et al.; 1998) that strong vertical isotope gradients in soil can exist. Enrichment does mainly occur in the upper soil layers, while water in deeper soil layers, which can be used for plant transpiration, is more depleted. Thus, a one-layer

GMDD
5, 3375–3418, 2012

bucked model will most likely result in too enriched isotope values of evaporated and transpired water. Furthermore, in a previous study, Schulz et al. (2000) analyzed the results of coupling the ECHAM model with various land surface schemes of different complexity. They showed that a bucket model tends to calculate higher evaporation amounts than more complex schemes. Such overestimation will result in a too strong influence of the isotopic composition of the soil water on the atmospheric isotopic composition, and consequently, on the isotopic values simulated in precipitation.

3.2.3 Sensitivity of kinetic fractionation

In order to examine the influence of the kinetic fractionation coefficient α_k of terrestrial evaporation on the isotopic composition, we use the model setup FE (fractionation occurring during evaporation only) extended by two calculations of the kinetic fractionation: for the first model setup (named $FEK_{openwater}$) we assume the same kinetic coefficient as over the ocean, which is presented in the study given by Merlivat and Jouzel (1979). The second setup ($FEK_{diffres}$) is based on the study given by Mathieu and Bariac (1996), where α_k is calculated as the nth power of the molecular diffusivity ratio. For the exponent n we use, as suggested by Riley et al. (2002), $n = 0.67$. As the third setup of the analyzes we use FE, which has no kinetic fractionation included.

When using the $FEK_{openwater}$ setup instead of the FE one, a slightly weaker depletion of the simulated $\delta^{18}O_{ws}$ (Fig. 14c) in the range of −1.3‰ to −0.3‰ is detected in the northern high latitudes. The difference between the simulated $\delta^{18}O_P$ of the $FEK_{openwater}$ and FE setup is negligible, with changes in the range of ±0.1‰ (Fig. 14a). The difference of the simulated $\delta^{18}O_{ws}$ of the FE and the $FEK_{diffres}$ setup (Fig. 14d) are more noticeable. The calculated $\delta^{18}O_{ws}$ of the $FEK_{diffres}$ setup is more depleted in the northern high latitudes and the Tibetan Plateau in comparison to FE in a range of 0.5‰ to 4.9‰. However, the anomaly of the simulated $\delta^{18}O_P$ of FE−$FEK_{diffres}$ (Fig. 14b) results in only minor changes in the range of −0.14‰ to +0.45‰.

GMDD
5, 3375–3418, 2012

Furthermore, we compare the simulated $\delta^{18}O_P$ values as well as the simulated relation of δD_P and the deuterium excess (defined as $dex_P = \delta D_P - 8\delta^{18}O_P$), with the observational data. For these studies we use again those 246 GNIP stations described in Sect. 2.3. Figure 15a depicts a comparison of the simulated annual mean $\delta^{18}O_P$ values with the observations. For all three model setups, the simulated $\delta^{18}O_P$ fits well with the observational values, but all three simulations overestimate the $\delta^{18}O_P$ for most of these GNIP stations. Moreover, Fig. 15a also shows that the calculated $\delta^{18}O_P$ is indistinguishable for the setups FE, $FEK_{openwater}$, and $FEK_{diffres}$. Figure 15b shows the simulated relation of δD_P and the deuterium excess (dex_P). It can be seen that the simulated $\delta D_P - dex_P$ relation behaves very similarly for all three setups and shows a similar distribution in comparison to the GNIP data.

The performed sensitivity test for the kinetic fractionation factor α_k reveals that the setups FE, $FEK_{diffres}$, and $FEK_{openwater}$ of the ECHAM5-JSBACH-wiso model simulate a different isotopic composition of the soil water. However, the simulations of $\delta^{18}O_P$ as well as at the simulation of the $\delta D_P - dex_P$ relation show no substantial difference between FE, $FEK_{diffres}$, and $FEK_{openwater}$.

4 Conclusions

In this study we show first simulation results of stable water isotopes successfully implemented in the coupled atmosphere land-surface model ECHAM-JSBACH. The ECHAM-JSBACH-wiso model is able to simulate the isotopic composition of precipitation ($\delta^{18}O_P$ and δD_P) in a comparable good manner as the stand-alone ECHAM5-wiso model. Furthermore we demonstrate that the relation between simulated temperature and $\delta^{18}O_P$ and between precipitation and $\delta^{18}O_P$, respectively, is simulated in good agreement with the observations.

An analysis of the impact of the coupling of ECHAM5 and JSBACH reveals that the simulated land surface temperature and surface albedo are highly influenced by

GMDD
5, 3375–3418, 2012

the coupled setup and lead to some substantial regional changes of the hydrological cycle between the model ECHAM5-JSBACH and the stand alone ECHAM5 model. This results in differences of the modeled soil wetness and evapotranspiration fluxes between the two models.

To investigate the importance of isotope fractionation processes over land surfaces, we use three different model setups. Our studies show that the best agreement of the ECHAM5-JSBACH-wiso results with the observational data from different GNIP stations is given, if no fractionation during evaporation and transpiration processes over land surface is assumed. This surprising result might be explained by the simplified representation of soil water as a one-layer bucket model in ECHAM5-JSBACH. It remains open how the isotopic result would change for a more complex multi-layer soil model.

In the future, we plan a set of Holocene simulations with the ECHAM5-JSBACH-wiso model, which will distinguish between prescribed and dynamic vegetation. By using the ECHAM5-JSBACH-wiso model with dynamical vegetation we are able to investigate the feedback mechanisms between the hydrological cycle and the vegetation during the past. Moreover, the new isotope diagnostics will give the opportunity to compare the simulated isotopic composition of ECHAM5-JSBACH-wiso with avaiable proxy data to improve our understanding of past hydrological changes. Furthermore, since the ocean model MPI-OM has also been enhanced with stable water isotopes (see Xu et al., 2012), we will be able to run simulations with a full coupled atmosphere-ocean-land-surface GCM including isotopes in the future.

Acknowledgements. This work is funded by Deutsche Forschungsgemeinschaft (DFG) as part of the project HYDRACENE (A new hydrogen-isotope approach to understand North African monsoon changes in the Holocene) within the framework of the Special Priority Programme INTERDYNAMIK.

GMDD
5, 3375–3418, 2012

References

Aleinov, I. and Schmidt, G. A.: Water isotopes in the GISS ModelE land surface scheme, Global Planet. Change, 51, 108–120, 2006. 3377, 3378

Allison, G. and Hughes, M.: The use of natural tracers as indicators of soil-watermovement in a temperate semi-arid region, J. Hydrol., 60, 157–173, doi:10.1016/0022-1694(83)90019-7, available at: http://www.sciencedirect.com/science/article/pii/0022169483900197 (last access: 25 September 2012), 1983. 3395

Brovkin, V., Raddatz, T., Reick, C. H., Claussen, M., and Gayler, V.: Global biogeophysical interactions between forest and climate, Geophys. Res. Lett., 36, L07405, doi:10.1029/2009GL037543, 2009. 3380

Craig, H. and Gordon, L. I.: Deuterium and oxygen 18 variations in the ocean and the marine atmosphere, in: Stable Isotopes in Oceanographic Studies and Paleotemperature, edited by: Tongiorgi, E., V. Lishi e F., Pisa, Italy, 9–130, 1965. 3383

Dansgaard, W.: Stable isotopes in precipitation, Tellus, 16, 436–468, doi:10.1111/j.2153-3490.1964.tb00181.x, 1964. 3376, 3387

DKRZ: The ECHAM3 atmospheric general circulation model, Tech. Rep. 6, Deutsches Klimarechenzentrum, Hamburg, Germany, 1992. 3380

Fischer, M. J.: iCHASM, a flexible land-surface model that incorporates stable water isotopes, Global Planat. Change, 51, 121–130, 2006. 3377, 3390

Gat, J. R.: Oxygen and hydrogen isotopes in the hydrologic cycle, Earth Planet Sc. Lett., 24, 225–262, doi:10.1146/annurev.earth.24.1.225, 1996. 3378, 3379

Herold, M. and Lohmann, G.: Eemian tropical and subtrobical African moisture transport: an isotope modelling study, Clim. Dynam., 33(7-8), 1075–1088, doi:10.1007/s00382-008-0515-2, 2009. 3378

Hoffmann, G., Werner, M., and Heimann, M.: Water isotope module of the ECHAM atmospheric general circulation model: a study on timescales from days to several years, J. Geophys. Res., 103, 871–896, 1998. 3377, 3378, 3380, 3381

Hsieh, J. C. C., Chadwick, O. A., Kelly, E. F., and Savin, S. M.: Oxygen isotopic composition of soil water: quantifying evaporation and transpiration, Geoderma, 82, 269–293, doi:10.1016/S0016-7061(97)00105-5, 1998. 3395

GMDD
5, 3375–3418, 2012

IAEA/WMO: Global Network of Isotopes in Precipitation: The GNIP Database, available at: http://www-naweb.iaea.org/napc/ih/index.html (last access: 24 October 2012), 2006. 3377, 3384

Joussaume, S., Sadourny, R., and Jouzel, J.: A general circulation model of water isotope cycles in the atmosphere, Nature, 311, 24–29, doi:10.1038/311024a0, 1984. 3377

Jouzel, J., Russell, G. L., Suozzo, R. J., Koster, R. D., White, J. W. C., and Broecker, W. S.: Simulations of the HDO and $H_2{}^{18}O$ atmospheric cycles using the NASA GISS general circulation model: the seasonal cycle for present-day conditions, J. Geophys. Res., 92, 739–760, doi:10.1029/JD092iD12p14739, 1987. 3377

Jouzel, J., Hoffmann, G., Kosterb, R. D., and Masson, V.: Water isotopes in precipitation: data/model comparison for present-day and past climates, Global Planet. Change, 19, 363–379, 2000. 3378

Knorr, W.: Annual and interannual CO_2 exchanges of the terrestria biosphere: process-based simulations and uncertainties, Global Ecol. Biogeogr., 9, 225–252, doi:10.1046/j.1365-2699.2000.00159.x, 2000. 3380

Lee, J.-E., Fung, I., DePaolo, D. J., and Henning, C. C.: Analysis of the global distribution of water isotopes using the NCAR atmospheric general circulation model, J. Geophys. Res., 112, D16306, doi:10.1029/2006JD007657, 2007. 3377

LeGrande, A. N. and Schmidt, G. A.: Global gridded data set of the oxygen isotopic composition in seawater, Geophys. Res. Lett., 33, L12604, doi:10.1029/2006GL026011, 2006. 3383

Majoube, M.: Fractionnement en oxygene 18 entre la glace et la vapeur d'eau, J. Chem. Phys., 68, 625–636, 1971a. 3382

Majoube, M.: Fractionnement en oxygene 18 et en deuterium entre l'eau et sa vapeur, J. Chem. Phys., 10, 1423–1436, 1971b. 3382

Mathieu, R. and Bariac, T.: A numerical model for the simulation of stable isotope profiles in drying soils, J. Geophys. Res., 101, 685–696, 1996. 3379, 3382, 3383, 3396

Merlivat, L. and Jouzel, J.: Global climatic interpretation of the deuterium-oxygen 18 relationship for precipitation, J. Geophys. Res., 84, 5029–5033, 1979. 3379, 3382, 3383, 3396

Noone, D. and Simmonds, I.: Associations between $d^{18}O$ of water and climate parameters in a simulation of atmospheric circulation for 197995, J. Climate, 15, 3150–3169, doi:10.1175/1520-0442(2002)015<3150:ABOOWA>2.0.CO;2, 2002. 3377

Raddatz, T. J., Reick, C. H., Knorr, W., Kattge, J., Roeckner, E., Schnur, R., Schnitzler, K.-G., Wetzel, P., and Jungclaus, J.: Will the tropical land biosphere dominate the cli-

GMDD

5, 3375–3418, 2012

matecarbon cycle feedback during the twenty-first century?, Clim. Dynam, 29, 565–574, doi:10.1007/s00382-007-0247-8, 2007. 3378, 3380

Riley, W. J., Still, C. J., Torn, M. S., and Berry, J. A.: A mechanistic model of $H_2^{18}O$ and $C^{18}O$ fluxes between ecosystems and the atmosphere: model description and sensitivity analyses, Global Biogeochem. Cy., 16, 1095, doi:10.1029/2002GB001878, 2002. 3396

Risi, C., Bony, S., Vimeux, F., and Jouzel, J.: Water-stable isotopes in the LMDZ4 general circulation model: model evaluation for present-day and past climates and applications to climatic interpretations of tropical isotopic records, J. Geophys. Res., 115, D12118, doi:10.1029/2009JD013255, 2010. 3377, 3378

Roeckner, E., Bäuml, G., Bonaventura, L., Brokopf, R., Esch, M., Giorgetta, M., Hagemann, S., Kirchner, I., Kornblueh, L., Manzini, E., Rhodin, A., Schlese, U., Schulzweida, U., and Tompkins, A.: Report No. 349 – The atmospheric general circulation model ECHAM5 – Part 1, Tech. rep., Max-Planck Inst. für Meteorol., Hamburg, Germany, 2003. 3378, 3380

Sachse, D., Billault, I., Bowen, G. J., Chikaraishi, Y., Dawson, T. E., Feakins, S. J., Freeman, K. H., Magill, C. R., McInerney, F. A., van der Meer, M. T. J., Polissar, P., Robins, R. J., Sachs, J. P., Schmidt, H.-L., Sessions, A. L., White, J. W., West, J. B., and Kahmen, A.: Molecular paleohydrology: interpreting the Hydrogen-Isotopic composition of lipid biomarkers from photosynthesizing organisms, Earth Planet. Sc. Lett., 40, 221–249, doi:10.1146/annurev-earth-042711-105535, 2012. 3390

Schmidt, G. A.: Oxygen-18 variations in a global ocean model, Geophys. Res. Lett., 25, 1201–1204, doi:10.1029/98GL50866, 1998. 3377

Schmidt, G. A., LeGrande, A. N., and Hoffmann, G.: Water isotope expressions of intrinsic and forced variability in a coupled ocean-atmosphere model, J. Geophys. Res., 112, D10103, doi:10.1029/2006JD007781, 2007. 3377

Schulz, J.-P., Dümenil, L., and Polcher, J.: On the land surface-atmosphere coupling and its impact in a single-column atmospheric model, J. Appl. Meteorol., 40, 642–663, 2000. 3396

Sturm, C., Zhang, Q., and Noone, D.: An introduction to stable water isotopes in climate models: benefits of forward proxy modelling for paleoclimatology, Clim. Past, 6, 115–129, doi:10.5194/cp-6-115-2010, 2010. 3377

Taylor, K. E., Williamson, D., and Zwiers, F.: The sea surface temperature and sea-ice concentration boundary conditions for AMIP II simulations, PCMDI Report No. 60, Tech. rep., Program for Climate Model Diagnosis and Intercomparison, Lawerence Livermore National Laboratory, Livermore, California, 25 pp., 2000. 3383

GMDD

5, 3375–3418, 2012

Tindall, J. C., Valdes, P. J., and Sime, L. C.: Stable water isotopes in HadCM3: isotopic signature of El Nino southern oscillation and the tropical amount effect, J. Geophys. Res., 114, D04111, doi:10.1029/2008JD010825, 2009. 3377

Vuille, M. and Werner, M.: Stable isotopes in precipitation recording South American summer monsoon and ENSO variability: observations and model results, Clim. Dynam., 25, 401–413, doi:10.1007/s00382-005-0049-9, 2005. 3378

Wang, K. and Dickson, R. E.: A review of global terrestrial evapotranspiration: observation, modeling, climatologie, and climatic variability, Rev. Geophys., 50, RG2005, doi:10.1029/2011RG000373, 2012. 3389

Werner, M., Langebroek, P., Carlsen, T., Herold, M., and Lohmann, G.: Stable water isotopes in the ECHAM5 general circulation model: towards high-resolution isotope modeling on a global scale, J. Geophys. Res., 116, D15109, doi:10.1029/2011JD015681, 2011. 3377, 3378, 3379, 3381, 3384, 3385, 3389

Xu, X., Werner, M., Butzin, M., and Lohmann, G.: Water isotope variations in the global ocean model MPI-OM, Geosi. Model Dev., 5, 809–818, doi:10.5194/gmd-5-809-2012, 2012. 3377, 3398

Yoshimura, K., Miyazaki, S., Kanae, S., and Oki, T.: Iso-MATSIRO, a land surface model that incorporates stable water isotopes, Glob. Planet. Change, 51, 90–107, 2006. 3377, 3390

GMDD

5, 3375–3418, 2012

Table 1. Pearson correlation coefficient R^2 of the relationship between observed $\delta^{18}O_p$ values and the by ECHAM5-JSBACH-wiso simulated $\delta^{18}O_p$ (δHDO_p) values.

Implementation	r^2 for $\delta^{18}O_p$	r^2 for δHDO_p
FE ($T \leq 20^{\circ}C$)	0.89	0.89
FEK ($T \leq 20^{\circ}C$)	0.89	0.9
FET ($T \leq 20^{\circ}C$)	0.89	0.89
noF ($T \leq 20^{\circ}C$)	0.9	0.91
FE ($T \geq 20^{\circ}C$)	0.71	0.68
FEK ($T \geq 20^{\circ}C$)	0.74	0.72
FET ($T \geq 20^{\circ}C$)	0.75	0.74
noF ($T \geq 20^{\circ}C$)	0.77	0.77

GMDD
5, 3375–3418, 2012

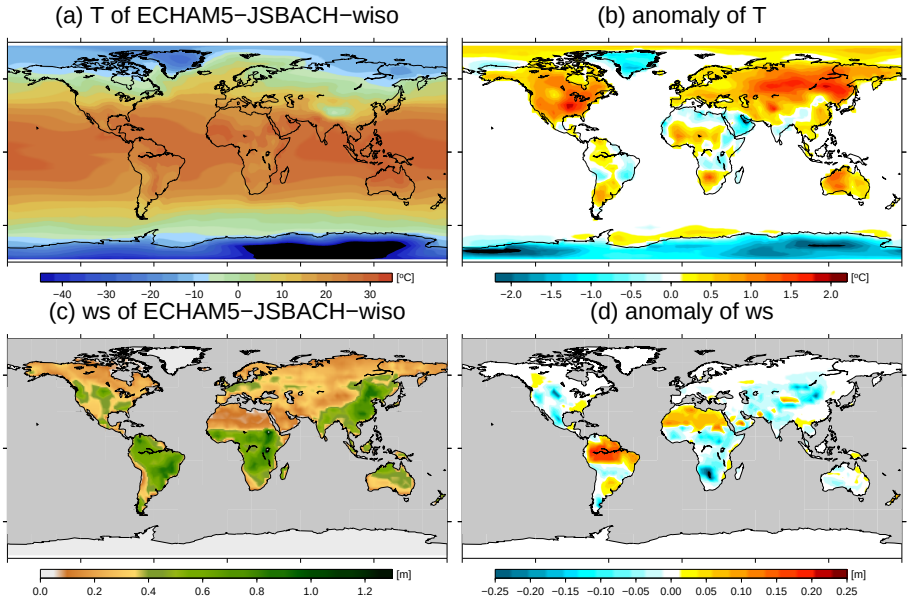

Fig. 1. Comparison of ECHAM5-JSBACH-wiso and ECHAM5-wiso at resolution T31L19: the annual mean values of **(a)** surface temperature (T), and **(c)** soil wetness (ws) as well as the anomaly between ECHAM5-JSBACH-wiso and ECHAM5-wiso **(b)** for temperature, and **(d)** for soil wetness.

GMDD
5, 3375–3418, 2012

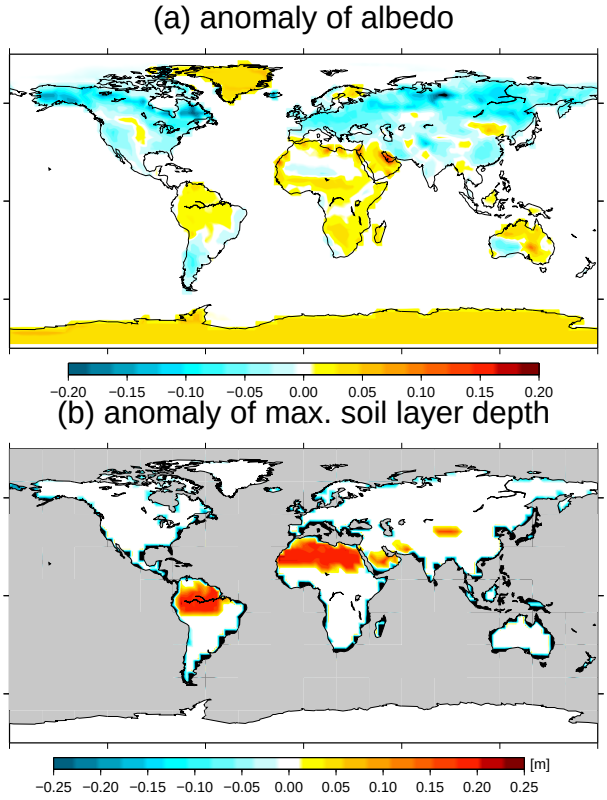

Fig. 2. Anomaly plot between ECHAM5-JSBACH-wiso and ECHAM5-wiso: **(a)** annual mean values of albedo, and **(b)** annual mean values of maximal soil layer depth.

GMDD
5, 3375–3418, 2012

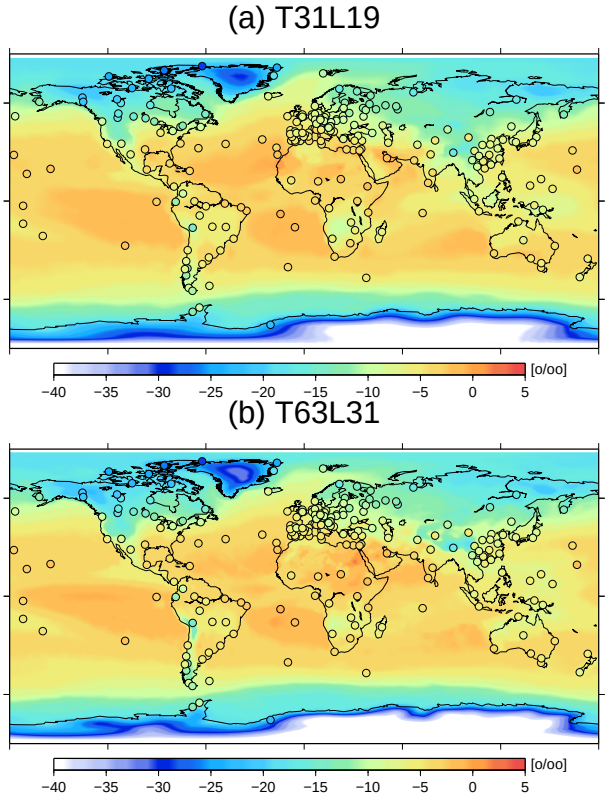

Fig. 3. Global map of observed $\delta^{18}O_P$ values (circles) and by ECHAM5-JSBACH-wiso simulated present-day annual mean $\delta^{18}O_P$ values (background map) for the resolutions **(a)** T31L19 and **(b)** T63L31.

GMDD
5, 3375–3418, 2012

Water isotopes in the atmosphere–land surface model ECHAM5-JSBACH

B. Haese et al.

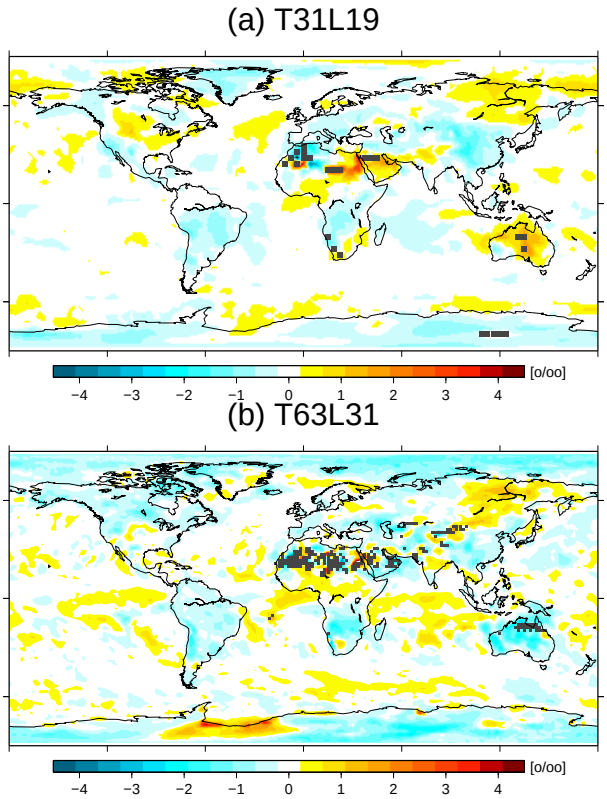

Fig. 4. Anomaly of ECHAM5-JSBACH-wiso (noF) – ECHAM5-wiso of annual mean $\delta^{18}O_P$ values for the resolutions **(a)** T31L19 and **(b)** T63L19. The gray areas in the figures mark those grid boxes where the simulated interannual variability is larger than 2‰.

GMDD
5, 3375–3418, 2012

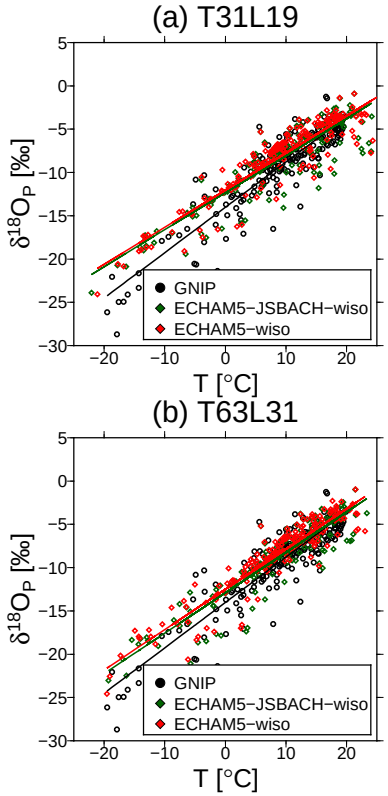

Fig. 5. Comparison of the simulated $\delta^{18}O_P$–T_{2m} relation of ECHAM5-JSBACH-wiso (noF) with ECHAM5-wiso observed for the resolutions **(a)** T31L19 and **(b)** T63L31. For comparison with the observed relation, we use data from those GNIP stations, where the annual mean temperature is below 20 °C.

GMDD
5, 3375–3418, 2012

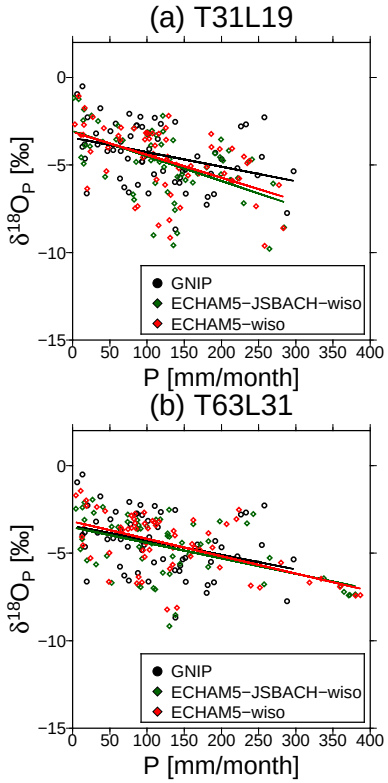

Fig. 6. Comparison of the simulated $\delta^{18}O_P$–P relation of ECHAM5-JSBACH-wiso (noF) with ECHAM5-wiso for the resolutions **(a)** T31L19 and **(b)** T63L31. For comparison with the observed relation, we use data from those GNIP stations, where the annual mean temperature is above or equal 20 °C.

GMDD
5, 3375–3418, 2012

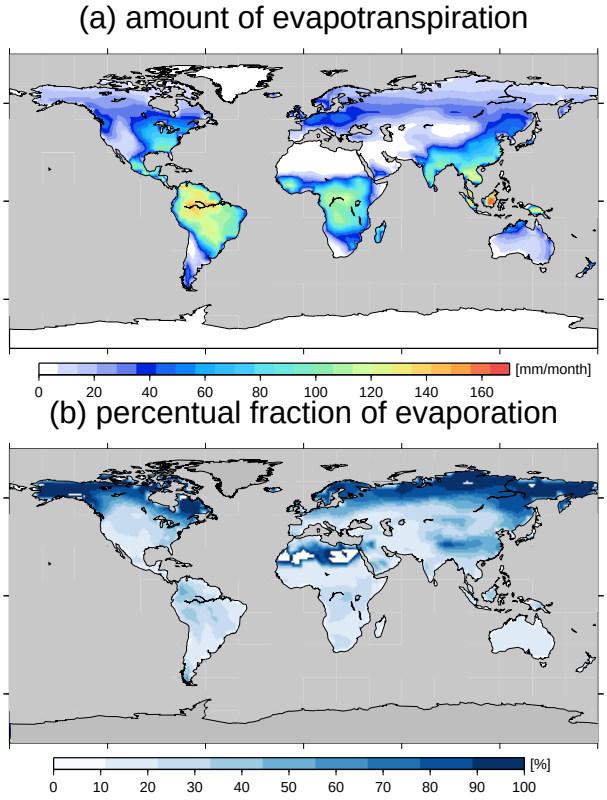

Fig. 7. Panel **(a)** shows the annual mean amount of evapotranspiration from land surface, and **(b)** the fraction of evaporation expressed as percentual amount of total evapotranspiration.

GMDD
5, 3375–3418, 2012

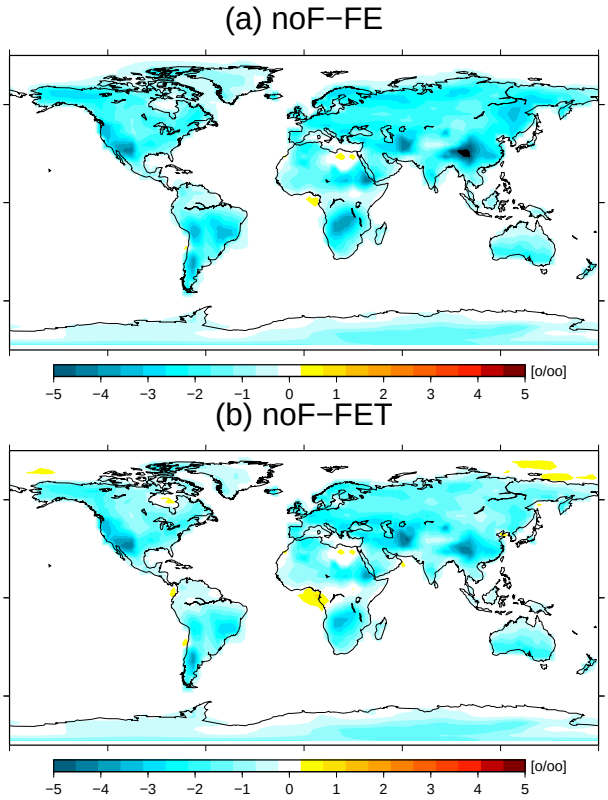

Fig. 8. Annual mean value of the simulated anomaly of $\delta^{18}O_P$ for **(a)** noF-FE, and **(b)** noF-FET.

GMDD
5, 3375–3418, 2012

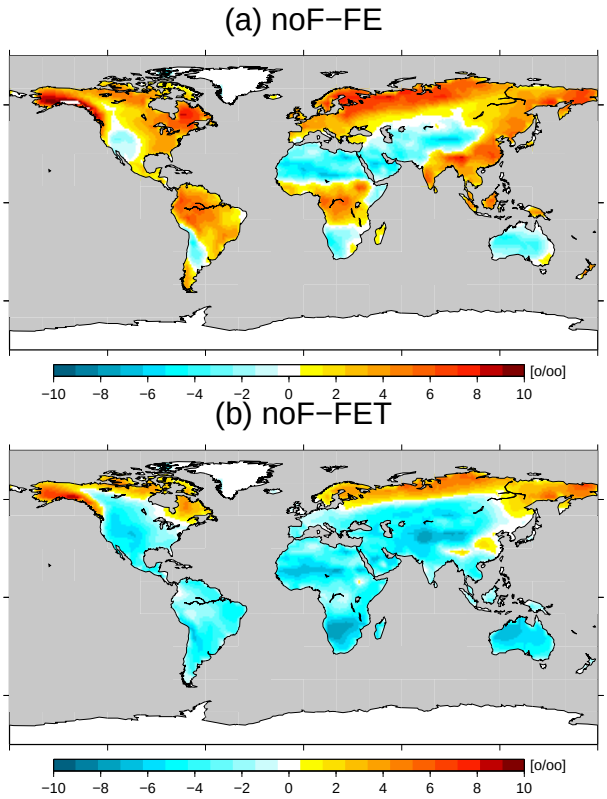

Fig. 9. Annual mean value of the simulated anomaly of $\delta^{18}O_{ws}$ for **(a)** noF-FE, and **(b)** noF-FET.

GMDD
5, 3375–3418, 2012

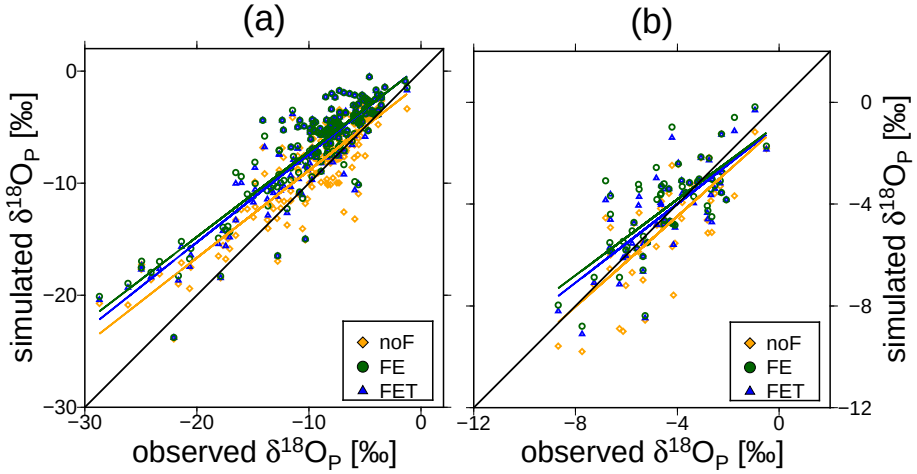

Fig. 10. Comparison of the by ECHAM5-JSBACH-wiso simulated and observational data of $\delta^{18}O_P$: **(a)** $T \leq 20^{\circ}C$ and **(b)** $T \geq 20^{\circ}C$.

GMDD
5, 3375–3418, 2012

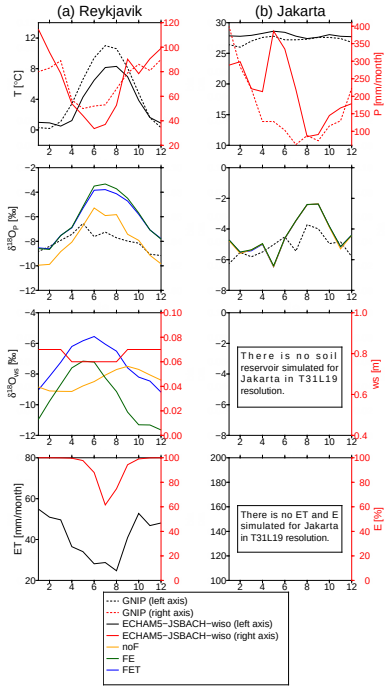

Fig. 11. Seasonal cycles of temperature T, precipitation amount P, isotopic composition of precipitation $\delta^{18}O_P$, isotopic composition of soil water $\delta^{18}O_{ws}$, depth of soil water ws, evapotranspiration from land surface ET, and fraction of evaporation E for the locations **(a)** Reykjavik, **(b)** Jakarta. The dotted lines represents the observational GNIP values (left = black, right = red). For the simulations the black/red lines represents the simulated T, P, E, ws and the fraction of evaporation. The simulated $\delta^{18}O$ values in precipitation and the soil reservoir are the yellow (noF), green (FE) and blue (FET) lines.

GMDD
5, 3375–3418, 2012

Water isotopes in the atmosphere–land surface model ECHAM5-JSBACH

B. Haese et al.

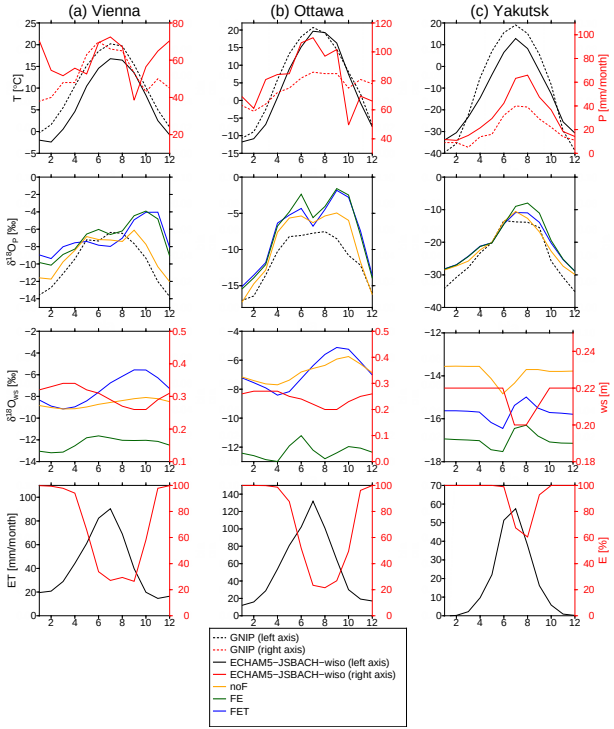

Fig. 12. As Fig. 11 for the locations **(a)** Vienna, **(b)** Ottawa, and **(c)** Yakutsk.

GMDD
5, 3375–3418, 2012

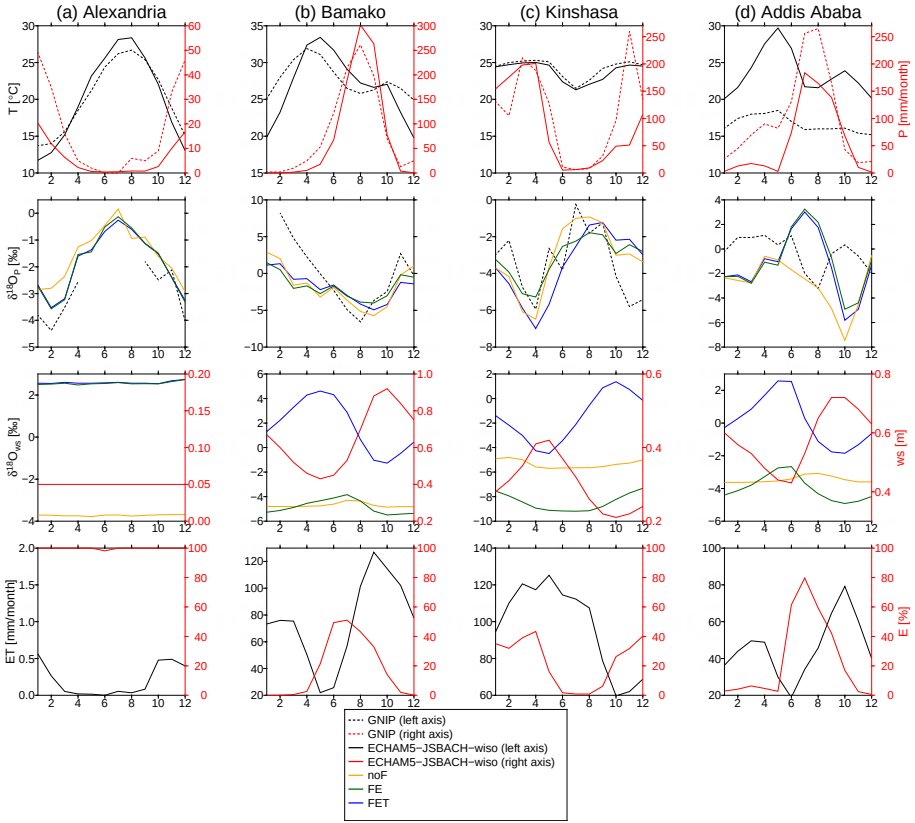

Fig. 13. As Figs. 11 and 12 for the locations **(a)** Alexandria, **(b)** Bamako, **(c)** Kinshasa, and **(d)** Addis Ababa.

GMDD
5, 3375–3418, 2012

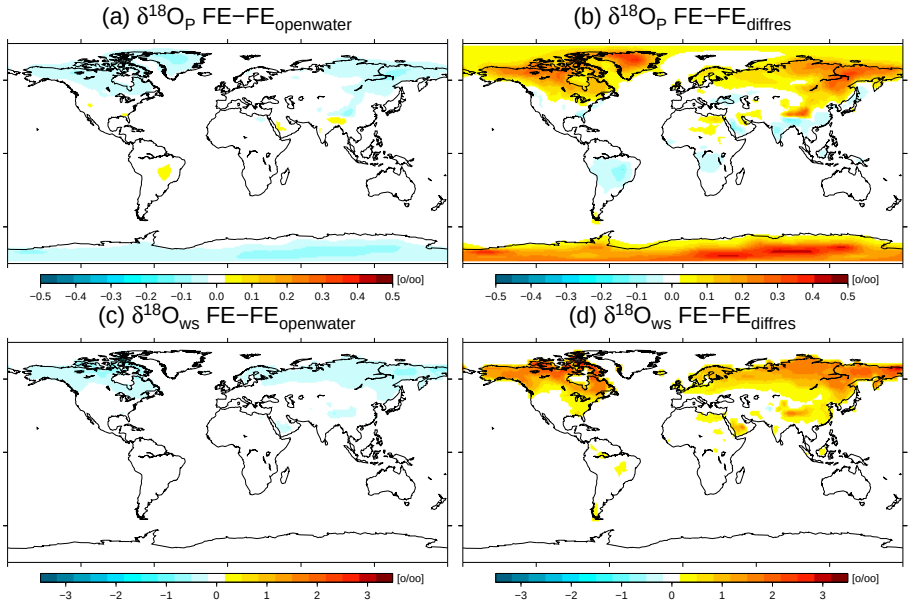

Fig. 14. Annual mean value of the simulated anomaly of $\delta^{18}O_P$ for **(a)** FE-FE$_{openwater}$, **(b)** FE-FE$_{diffres}$, and of $\delta^{18}O_{ws}$ **(c)** FE-FE$_{openwater}$, **(d)** FE-FE$_{diffres}$.

GMDD
5, 3375–3418, 2012

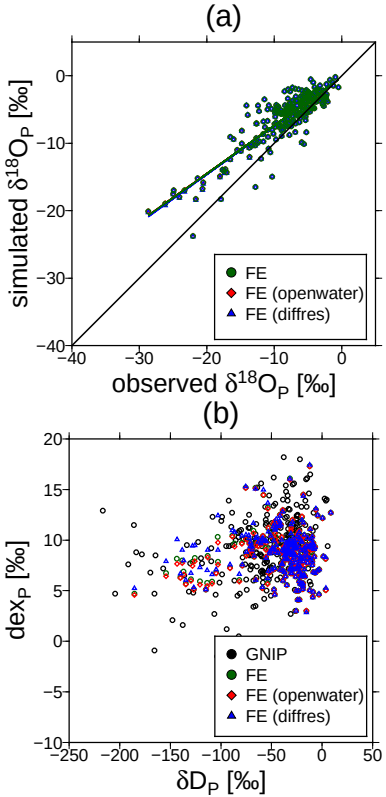

Fig. 15. Comparison of the kinetic fractionation factor for temperature below 20°C: **(a)** comparison of simulated and observed $\delta^{18}O_P$, and **(b)** relationship between deuterium excess in precipitation (dex_P) and δD_P.

GMDD
5, 3375–3418, 2012